

LASER TECHNOLOGIES

PACS numbers: 42.55.Wd; 42.55.Lt; 42.62.Cf
DOI: 10.1070/QE2014v044n03ABEH015320

High-quality laser cutting of stainless steel in inert gas atmosphere by ytterbium fibre and CO_2 lasers

A.A. Golyshev, A.G. Malikov, A.M. Orishich, V.B. Shulyat'ev

Abstract. **Processes of cutting stainless steel by ytterbium fibre and CO_2 lasers have been experimentally compared. The cut surface roughnesses for 3- and 5-mm-thick stainless steel sheets are determined. The absorption coefficient of laser radiation during cutting is measured. It is established that the power absorbed by metal during cutting by the CO_2 laser exceeds that for the ytterbium laser (provided that the cutting speed remains the same). The fact that the maximum cutting speed of the CO_2 laser is lower than that of the ytterbium fibre laser is explained.**

Keywords: *laser cutting, CO_2 laser, ytterbium fibre laser, cut roughness, cutting speed, power efficiency.*

1. Introduction

The range of application of fibre and disk lasers in cutting metals constantly increases. These lasers have a number of advantages over conventional CO_2 lasers. To date, there are some experimental data on cutting various metals by solid-state lasers with a wavelength of 1 μm (a detailed review of studies on this subject can be found in [1]). It has been reliably established that, when cutting is performed in inert gas atmosphere, solid-state lasers yield a much higher (by a factor of 3–4) cutting speed of thin (1–2 mm) sheets than CO_2 lasers, provided that the laser power is the same [2, 3]. This advantage is less pronounced for sheets thicker than 3–4 mm and disappears for sheets 10 mm thick. Note that cutting of thick sheets by a CO_2 laser provides a better edge quality. Cutting can be limited in speed or stopped for the following two reasons: (i) insufficient input power and (ii) low rate of melt removal and cut sealing [4]. The latter occurs at high cutting speeds (more than 10–15 m min^{-1}) [4]. The difference in the cutting speeds for the two types of lasers is generally explained in terms of energy concepts and related to the difference in the Fresnel absorption at the cut front for radiations with wavelengths $\lambda = 1$ and 10 μm [5]. Within the known mathematical models of laser cutting, the formation of a cut front and absorption of radiation at this front are calculated disregarding the influence of melt (see, for example, [5–7]). Depending on the melt film parameters and the character of melt flow, the real shape of the front and the cut lateral surface may differ significantly from that calculated for the ideal case [8, 9]. To date, there are no theoretical models of laser cutting that would completely and adequately describe the hydrodynamic phenomena occurring during cut channel formation. In this context, it is important to perform a comparative experimental study of the characteristics of cuts obtained by lasers of two types [1, 8].

It should be emphasised that the cutting parameters in the majority of theoretical and experimental studies were chosen disregarding the cut quality, whereas the roughness of the cut surface as a quality factor is most important for many applications; sometimes the degree of roughness is used as a synonym of quality [10]. As was noted in [10], the increase in the thickness of sheets cut by solid-state lasers with conservation of a high cut quality (at the level provided by CO_2 lasers) is currently one of the main directions aimed at improving the laser cutting technique. Therefore, it is of interest to perform a comparative study of the cut characteristics, with a maximum cut quality attainable for each type of lasers. We performed optimisation in [11, 12] and measured the energy balance at minimum roughness for laser-oxygen cutting of low-carbon steel using a CO_2 laser in [13]. As far as we know, similar studies on cutting stainless steel in inert gas atmosphere for fibre lasers, in contrast to CO_2 lasers, have not been performed. For example, when measuring the cutting energy balance, Scintilla et al. [1] tried to provide identical initial parameters for lasers of two types. However, optimal parameters for lasers of one type can be nonoptimal for lasers of another type, and the results of these measurements may differ significantly from the results obtained under conditions of minimum roughness.

Cutting in inert gas atmosphere differs significantly from laser-oxygen cutting: the additional energy source in the form of exothermic oxidation reaction is absent, and the fracture of material at the cut front and the cut front propagation occur via other mechanisms. Therefore, the determination of the energy balance and conditions for obtaining a high-quality cut for laser cutting in inert gas atmosphere calls for a separate investigation. The purpose of our study was to perform a comparative experimental estimation of the energy balance and determine the cutting speeds of stainless steel by fibre and CO_2 lasers, provided that the cut surface roughness is reduced to minimum.

2. Schematics of the experiment

Cutting was performed by an IPG/IRE-Polus ytterbium fibre laser with a collimator (IPG, model D5-WC/AC), having a power of 2 kW and a beam parameter product BPP = 3.8 mm mrad. The beam diameter on the focusing lens after

A.A. Golyshev, A.G. Malikov, A.M. Orishich, V.B. Shulyat'ev
S.A. Khristianovich Institute of Theoretical and Applied Mechanics, Siberian Branch, Russian Academy of Sciences, ul. Institutskaya 4/1, 630090 Novosibirsk, Russia; e-mail: shulyat@rambler.ru

Received 4 October 2013; revision received 25 December 2013
Kvantovaya Elektronika **44** (3) 233–238 (2014)
Translated by Yu.P. Sin'kov

the collimator was 17 mm at a lens focal distance of 200 mm. We also used a CO_2 laser [14, 15] with a self-filtering cavity, characterised by a power up to 8 kW and BPP = 4.7 mm mrad. The beam diameter on the focusing lens was 25 mm at a focal length of 127 mm. The radiation intensity distribution in the lens focus is close to Gaussian. The diameter of the focused beam in the waist was estimated as the sum of the diffraction diameter and the diameter of the scattering circle caused by the spherical aberration. The total diameter was calculated to be 180 μm for the fibre laser and 160 μm for the CO_2 laser.

Square samples were cut from sheets of X12CrNiTi 18-9 stainless steel, with a nitrogen pressure in the cutter of 1.3–1.6 MPa. All measurements were performed at a laser power of 2 kW. Sheets of stainless steel 3 and 5 mm in thickness were used. For these thicknesses we investigated the surface roughness as a function of the cutting speed; at each speed value the waist position was optimised according to the criterion of minimum roughness for each laser.

The roughness measure (characteristic height of inhomogeneities) was chosen to be the arithmetic mean of profile deviation, R_a; it was measured using an Olympus LEXT confocal laser scanning microscope. To determine the energy balance, we found the absorption coefficients of laser radiation during metal cutting according to the technique described in detail in [16]; it was used to analyse the energy balance for cutting by a CO_2 laser beam in oxygen atmosphere [11–13]. The transmitted radiation arrived at a detector (OPHIR 5000W-CAL-SH meter power).

The absorption coefficient is considered to be an integral parameter, which also takes into account the power of radiation absorbed during possible multiple reflections from the cut front and walls: $A = (W - W_{tr})/W$, where W is the laser power before the focusing lens and W_{tr} is the power of the radiation transmitted through the cut channel. The size and deviation of the laser beam interacting with the material during cutting were specially controlled to make all radiation transmitted through the cut region arrive at the detector. The melt particles removed from the cut region were blown away by an air jet to exclude their arrival at the detector.

3. Experimental results

Figure 1 shows photographs of typical cross sections of the cut channel and cut surface for stainless steel specimens irradiated by an ytterbium fibre laser with $\lambda = 1.07$ μm and a gas-discharge CO_2 laser with $\lambda = 10.6$ μm. A detailed study of the cut surface roughness was performed for sheet thicknesses h = 3 and 5 mm. To this end, we measured the roughness R_a along a 3-mm-long line oriented parallel to the sheet surface. The roughness was determined in 26 cross sections; for example, for the sheet with h = 3 mm, the measurements were performed with an interval of 120 μm. Typical measurement results are shown in Fig. 2. It can be seen that the character of depth distribution of roughness R_a is different for lasers of different types; however, the depth distribution is highly nonuniform, with a maximum-to-minimum ratio of almost 2. Note the enhanced roughness in the lower part of the cut made by the CO_2 laser.

The above results demonstrate clearly that a comparison of the cuts in roughness at separate points along the cut channel height may lead to incorrect conclusions; hence, one must use R_a values averaged over the entire plate thickness. The data on the average roughness, obtained by optimising the

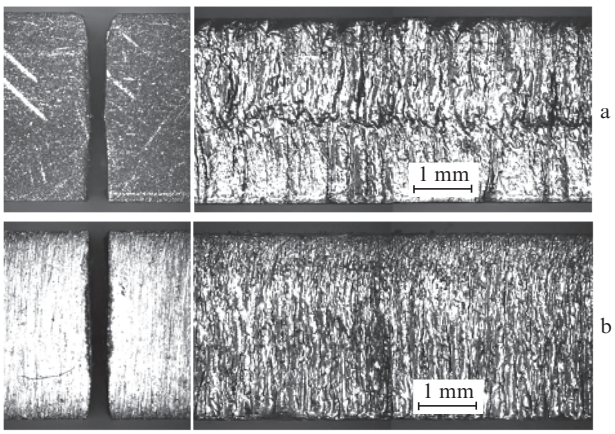

Figure 1. Cut channel cross sections and cut surfaces for cutting by (a) CO_2 and (b) fiber lasers (h = 3 mm, W = 2 kW).

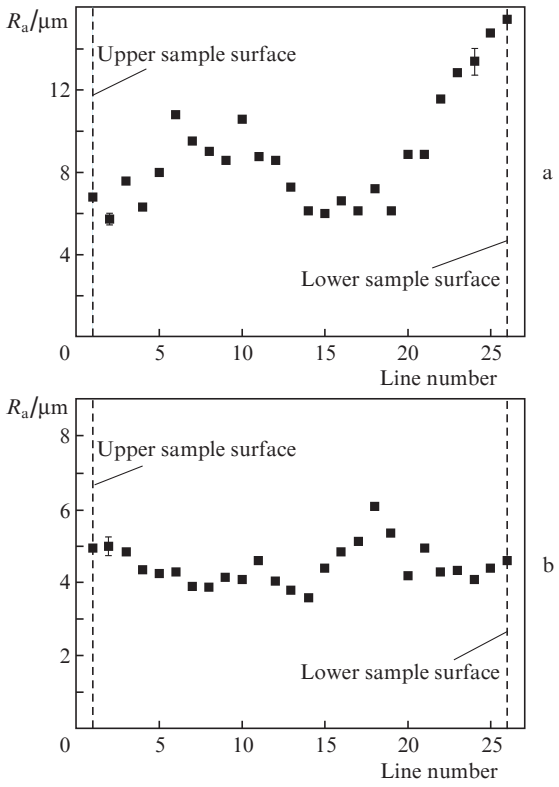

Figure 2. Values of surface roughness R_a at different distances from the sample surface for (a) CO_2 (cutting speed V_c = 1.5 m min^{-1}) and (b) fibre (V_c = 3 m min^{-1}) lasers.

position of the focus with respect to the sheet surface for each cutting speed V_c, are shown in Fig. 3 for h = 3 and 5 mm. It can be seen that the average roughness is larger at low speeds; it decreases with increasing speed to some value and then remains constant up to the maximum (critical) speed, after which cutting becomes impossible. The critical cutting speeds V_c^{cr} are listed in Table 1.

It is noteworthy that the average roughnesses (measured for the optimal focus position and identical cutting speeds) are similar for both types of lasers; however, the limiting cutting speed for the fibre laser exceeds that for the CO_2 laser by a factor of almost 1.5–2 (see Table 1).

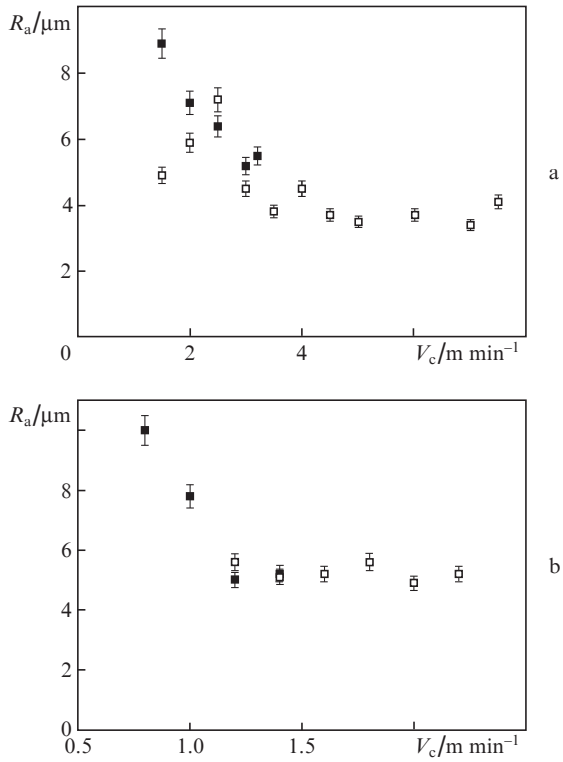

Figure 3. Dependences of the roughness (averaged over the plate thickness) on the cutting speed at h = (a) 3 and (b) 5 mm for cutting by (filled squares) CO_2 and (open squares) fibre lasers.

Table 1. Critical cutting rates for stainless steel.

Laser type	h/mm	V_c^{cr}/m min^{-1}
CO_2 laser	3	3.2 ± 0.05
	5	1.4 ± 0.05
Fibre laser	3	7.5 ± 0.05
	5	2.2 ± 0.05

The specific features of the cut structure at cutting speeds close to critical were investigated by an example of cutting a 3-mm-thick plate with the CO_2 laser. Figure 4 shows a photograph of a cut lap and a dependence of the cut width on the upper sheet surface, b_{up}, on the cutting speed for cutting a plate with a thickness h = 3 mm by the CO_2 laser. The data obtained both for cutting in the optimal mode at a speed below critical and for higher cutting speeds are presented. Note that in some cases the melt was removed from the channel by a gas flow (Fig. 4); however, 'sealing' of the channel was observed more often. Cut channel laps, similar to those presented in Fig. 1, were prepared to determine the cut width. The cut width b_{up} was measured at the input of the channel and the average cut width b_{av} was found from the relation $b_{av} = S/h$, where S is the channel cross section area. To determine the area S, we prepared laps of cut cross sections for each sample. Note that the b_{up} value is much larger than b_{av} in the case of cutting by the CO_2 laser; it can be seen well in Fig. 1b. However, when the cutting speed reaches the critical value (Fig. 4), a kink in the dependence $b_{up}(V_c)$ and a sharp decrease in b_{up} are observed.

Figure 5 shows the absorption coefficient A as a function of the cutting speed for the fibre and CO_2 lasers and plate thicknesses h = 3 and 5 mm. Note that the A values are much

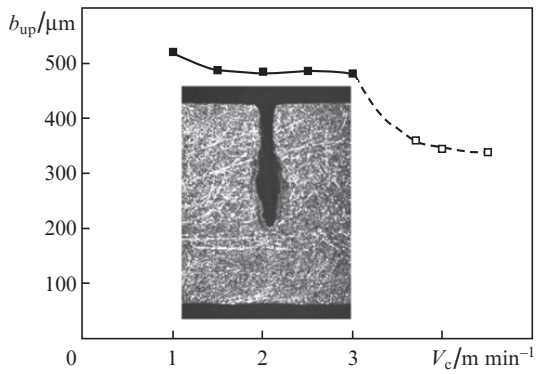

Figure 4. Cut width on the sheet upper surface, b_{up}, for cutting a 3-mm thick sheet of stainless steel by CO_2 laser as a function of the cutting speed V_c: (solid line) high-quality cut and (dashed line) cutting at a speed exceeding critical. The photograph shows a cut channel lap at V_c = 4 m min^{-1}.

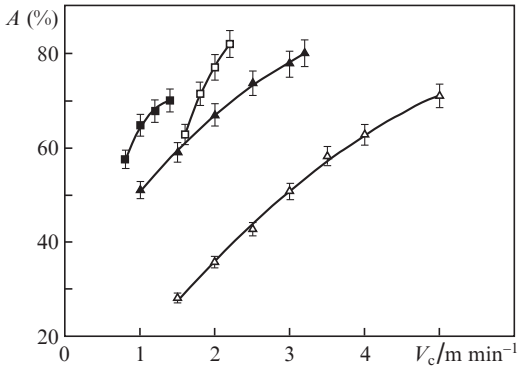

Figure 5. Dependences of the absorption coefficient of laser radiation on the cutting speed for (filled symbols) CO_2 and (open symbols) fibre lasers at h = (▲,△) 3 and (■,□) 5 mm.

larger for the CO_2 laser in comparison with that for the fibre laser (at the same cutting speed).

The measured average cut widths for h = 3 and 5 mm allowed us to determine the main optimal energy parameters: the Peclet number $Pe = (V_c b_{av})/\gamma$, where γ = 5.7 mm^2 s^{-1} is the thermal diffusivity of material, and the absorbed energy density $G = AW/(V_c b_{av} h)$ per melt unit volume. The results are

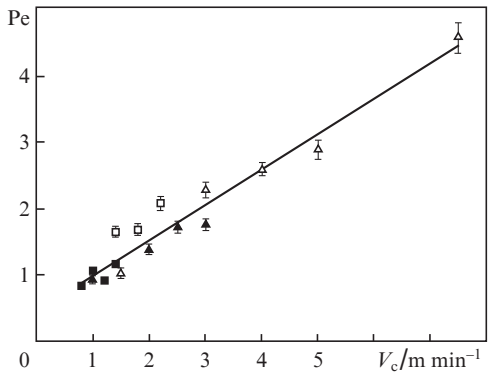

Figure 6. Dependences of the Peclet number on the cutting speed for (filled symbols) CO_2 and (open symbols) fibre lasers at h = (▲,△) and (■,□) 5 mm.

shown in Figs 6 and 7. One can see that the Peclet numbers for cutting by different lasers are similar, independent of the sheet thickness, and increase with increasing cutting speed. The density of the absorbed energy in the case of cutting by the fibre laser (with optimisation according to minimum roughness) barely depends on the cutting speed and sheet thickness. The energy density G for the fibre laser in the range of speeds from 1.5 to 5 m min^{-1} (Fig. 7) and $h = 3$ and 5 mm ranges from 26 to 32 J mm^{-3}. In the case of cutting by the CO_2 laser, the energy density spread is much higher: 42–66 J mm^{-3}. The average energy density for cutting by the CO_2 laser turned out to exceed the corresponding value for the fibre laser by a factor of about 2.

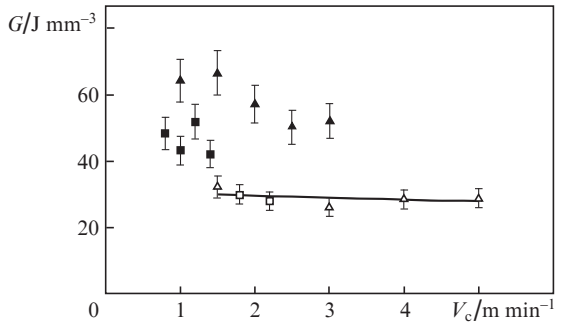

Figure 7. Dependences of the absorbed energy density G on the cutting speed for (filled symbols) CO_2 and (open symbols) fibre lasers at h = (▲,△) 3 and (■,□) 5 mm.

4. Discussion

To obtain a more complete and interrelated physical pattern of the laser cut formation, we will consider the cutting energy balance using nitrogen as an assisted gas. The balance equation is given by the well-known expression [1, 8]

$$AW = W_m + W_{cond} + W_{etc}, \quad (1)$$

where W_m is the power spent on heating and melting the metal; W_{cond} is the power lost from the cut region to the surrounding material due to the thermal conductivity; and W_{etc} takes into account the other losses of absorbed radiation power, including the loss on convective and radiative cooling. The W_m value can be calculated from the expression

$$W_m = V_c h b_{av}[\rho_m c_m(T_m - T_0) + \rho_m L_m + \rho_g c_g(T^* - T_m)], \quad (2)$$

where c_m, ρ_m and c_g, ρ_g are, respectively, the average specific heats and densities of the metal and melt during cutting; L_m is the heat of fusion; $T_m - T_0$ is the change in the metal temperature during cutting prior to the melting onset; and $T^* - T_m$ is the change in the melt temperature. The first term in (2) is the power spent on heating the metal to the melting temperature, the second term is the power spent on melting, and the third term is the power spent on heating the melt to a temperature of T^*.

To estimate the thermal losses, we will use the relation [17]

$$W_{cond} = 3.2\lambda_m h(T^* - T_m)\mathrm{Pe}^{0.868}, \quad (3)$$

where λ_m is the thermal conductivity of the material. Substituting (2) and (3) into (1) and neglecting the other power loss [1], we obtain a general expression for the absorbed energy density:

$$\frac{AW}{V_c h b_{av}} = \rho_m L_m + [\rho_m c_m(T_m - T_0) + \rho_g c_g(T^* - T_m)] + \frac{1.6\rho_m c_m(T^* - T_0)}{\mathrm{Pe}^{0.132}}. \quad (4)$$

Note that the Peclet number Pe was calculated in [17] using the channel half-width. Here, we determine the Peclet number based on the total channel width; therefore, when expressions (3) and (4) are used, the experimental Pe values must be reduced by a factor of 2.

It follows from (4) that the absorbed energy density depends very weakly on the Peclet number and is determined by a single parameter: T^*, i.e., the degree of melt overheating. The data in Fig. 6 indicate that the Peclet numbers at the maximum cutting speed are similar for both types of lasers. The absorbed energy density, according to the data in Fig. 7, is much higher for the CO_2 laser than for the fibre laser. According to (4), this means that the melt must be significantly superheated and contain excess energy; however, the experiment showed that cutting stopped in this case. Using $\rho_m = \rho_g = 7900$ kg m^{-3}, $c_m = c_g = 596$ J kg^{-1} K^{-1}, and $L_m = 276$ kJ kg^{-1} for estimation, we obtain the change in temperature from (4) to be $T^* - T_0 = 1800$ °C for the fibre laser at a characteristic density of absorbed energy $G = 28$ J mm^{-3} and Peclet number Pe = 2.5. However, when cutting by the CO_2 laser, the energy density $G = 57$ J mm^{-3} and Peclet number Pe = 1.37 correspond to $T^* - T_0 = 3600$ °C. Thus, the energy balance equations (1)–(4), which are generally used to determine the maximum cutting speed, yield a realistic estimate of the melt temperature in the case of the fibre laser. However, in the case of the CO_2 laser, the melt temperature obtained from (4) significantly exceeds the boiling temperature of the material and is obviously overestimated for cutting in the melting mode. This can be related to the significantly overestimated (for the CO_2 laser) absorption coefficient, measured as the relative difference in the powers before the focusing lens and at the output of the cut channel, when the possible reflection from the sheet surface is disregarded [16].

Let us consider a radically different approach to the problem of a lower critical cutting speed for the CO_2 laser in comparison with the cutting by the fibre laser. It is based on the suggestion that the processes occurring on the surface of a steel sheet (i.e., initiation and formation of a cut channel) play a key role. The spatial propagation of the cut front is a cyclic process [18, 19]. When a current cycle begins, the head of the laser beam, which is incident on the surface portion before the cut front at an angle close to 90°, heats and melts the material. Then the melting front penetrates into the bulk of the material to form the cut channel. Thus, a necessary condition for initiating a cut channel in each cycle is the heating of the sheet surface before the cut front to the melting temperature.

It is rather difficult to estimate the temperature of the cut surface because there are no reliable data on the absorption coefficient for a normally incident laser beam. The absorption coefficient depends strongly on the surface roughness, purity, presence of oxides, etc. In particular, this problem was considered in detail in monograph [20]. However, the following generalised result was obtained in [20]: the absorption of CO_2

laser radiation by stainless steel is much lower than that of the ytterbium fibre laser. For example, according to the data of [20], the absorption coefficient is 2%–5% for $\lambda = 10.6$ μm at room temperature and increases to 10% upon heating to 1000 °C, whereas the absorption coefficient for $\lambda = 1.07$ μm is ~30% and depends weakly on temperature.

To estimate the surface temperature before the cut front, we used the relation derived in [21] for the surface temperature of a semi-infinite body heated by a surface thermal source with a constant intensity:

$$T = \frac{2q}{\lambda_m}\sqrt{\frac{\gamma\Delta t}{\pi}}, \quad (5)$$

where Δt is the switch-on time of the source and q is the heat flow density. The surface temperature upon heating by a moving source can be estimated using the relation for an stationary pulsed source, assuming the pulse duration to be the ratio of the characteristic size of the source to its motion velocity [22]. We assume that heating of the sheet surface before the cut front occurs not over the entire focused-beam spot of radius r_f but only in a part of size ξr_f along the motion direction ($\xi < 1$). Then $\Delta t = \xi r_f / V_c$ and the expression for the temperature of the surface area sheet before the cut front has the form

$$T = \frac{4AW}{\pi b^2 \lambda_m}\sqrt{\xi\frac{2\gamma b}{\pi V_c}}, \quad (6)$$

where $q = AW/(\pi r_f^2)$; $b = 2r_f$.

The ξ value should not be too large for the following reason: to form a continuous cut of high quality, the main fraction of the beam power should be absorbed at the cut front inside the channel. Figure 8 shows the surface temperatures calculated from formula (6) at $\xi = 0.1$, using our data on the optimal cut width and the data of [20] on the absorption coefficient for a normally incident beam. The grey region corresponds to the conditions for cutting by the CO_2 laser. It can be seen that this region is crossed by the line $T = 1500$ °C, which corresponds to the melting temperature at speeds close to critical. Thus, due to the small absorption coefficient in the case of cutting by the CO_2 laser in inert gas atmosphere, the surface temperature is close to the melting temperature and decreases with an increase in the cutting speed, thus restricting the limiting cutting speed. A radically different situation is observed when the surface temperature is calculated for cutting by a fibre laser. Obviously overestimated temperatures were obtained for laser cutting of steel under same conditions and $\xi = 0.1$. This means that a temperature characteristic of laser cutting not exceeding the metal boiling temperature can be attained at a smaller ξ value: fibre laser radiation provides more efficient heating of the metal surface. The cutting speed of the CO_2 laser is limited by the insufficiently high surface heating, whereas this limitation is absent for the fibre laser. An indirect confirmation of this limitation for the CO_2 laser is the decrease in the cut channel width (see Fig. 4), i.e., the increase in ξ at cutting speeds exceeding critical: most of power is spent on heating the surface for initiating a channel.

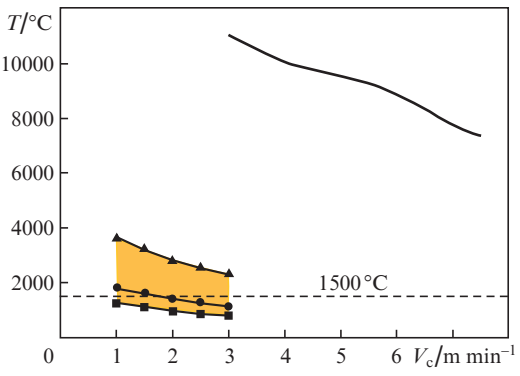

Figure 8. Dependences of the surface temperature on the cutting speed, calculated from formula (6), for (symbols) CO_2 and (solid line) fibre lasers at $h = 3$ mm and $A =$ (■) 3.5%, (●) 5%, (▲) 10%, and (solid line) 30%.

5. Conclusions

Based on the experimental study of the energy balance of stainless steel cutting by fibre and CO_2 laser beams, we revealed the main physical processes determining the cut quality and limiting the maximum cutting speed. It was established that, when cutting is performed with a minimum roughness, the cut width and Peclet number are independent of the laser wavelength (laser type) and determined by only the cutting speed.

It was shown that the limitation of the maximum cutting speed by fibre and CO_2 lasers can be caused by different physical factors. When cutting by the CO_2 laser in inert gas atmosphere, the reflection from the surface plays a significant role and limits the maximum cutting speed. In this case, the conventional methods for measuring the absorption coefficient [1, 13, 16], which disregard the reflection from the upper surface, may yield overestimated values. These methods are efficient for laser cutting in the presence of oxygen as an auxiliary gas, when the cut width generally exceeds the laser beam diameter, and the presence of the oxide film increases the absorption coefficient. In the case of cutting in inert gas atmosphere, these methods may lead to overestimation of the absorbed energy density and melt temperature. Specifically this circumstance explains the unreasonably high temperatures for cutting by the CO_2 laser; these values (noted in [1]), were calculated from formula (6).

Based on the results of this study, we concluded that the speed of high-quality cut is limited by the decrease in melt temperature and rise in the melt viscosity with an increase in the cutting speed, which hinders efficient removal of the melt. This conclusion is in agreement with the results of Scintilla et al. [1], who reported a higher melt viscosity in the case of cutting by a fibre laser in comparison with cutting by a CO_2 laser.

References

1. Scintilla L.D., Tricarico L., Wetzig A., Beyer E. *Int. J. Mach. Tools Manuf.*, **69**, 30 (2013).
2. Powell J., Kaplan A.F.H. *Proc. 31th Int. Congress on Applications of Lasers & Electro-Optics ICALEO-2012* (Anaheim, CA, USA, 2012) p. 277.
3. Himmer T., Pinder T., Morgenthal L., Beyer E. *Proc. 26th Int. Congress on Applications of Lasers & Electro-Optics ICALEO-2007* (Orlando, FL, USA, 2007) p. 87.
4. Olsen F.O. *Proc. 25th Int. Congress on Applications of Lasers & Electro-Optics ICALEO-2011* (Scottsdale, AZ, USA, 2006) p. 188.
5. Mahrle A., Beyer E. *J. Phys. D: Appl. Phys.*, **42**, 175507 (2009).
6. Niziev V.G., Nesterov A.V. *J. Phys. D: Appl. Phys.*, **32**, 1455 (1999).
7. Zaitsev A.V., Kovalev O.B., Smirnova E.M. *Dokl. Vseros. konf. 'Vzaimodeistvie vysokokontsentrirovannykh potokov energii s*

materialami v perspektivnykh tekhnologiyakh i meditsine' (Proc. All-Russia Conf. 'Interaction of Concentrated Energy Fluxes with Materials in Promising Technologies and Medicine') (Novosibirsk, 2011) p. 94.
8. Scintilla L.D., Tricarico L., Mahrle A., Wetzig A., Himmer T., Beyer E. *Proc. 29th Int. Congress on Applications of Lasers & Electro-Optics ICALEO-2010* (Anaheim, CA, USA, 2010) p. 249.
9. Hirano K., Fabbro R. *J. Laser Appl.*, **24**, 012006 (2012).
10. Poprawe R., Schulz W., Schmitt R. *Phys. Procedia*, **5**, 1 (2010).
11. Malikov A.G., Orishich A.M., Shulyat'ev V.B. *Kvantovaya Elektron.*, **39**, 547 (2009) [*Quantum Electron.*, **39**, 547 (2009)].
12. Malikov A.G., Orishich A.M., Shulyatyev V.B. *Int. J. Mach. Tools Manuf.*, **49**, 1152 (2009).
13. Malikov A.G., Orishich A.M., Shulyat'ev V.B. *Kvantovaya Elektron.*, **42**, 640 (2012) [*Quantum Electron.*, **42**, 640 (2012)].
14. Afonin Yu.V., Golyshev A.P., Ivanchenko A.I., Malov A.N., Orishich A.M., Pechurin V.A., Filev V.F., Shulyat'ev V.B. *Kvantovaya Elektron.*, **34**, 307 (2004) [*Quantum Electron.*, **34**, 307 (2004)].
15. Malikov A.G., Orishich A.M., Shulyat'ev V.B. *Kvantovaya Elektron.*, **39**, 191 (2009) [*Quantum Electron.*, **39**, 191 (2009)].
16. Miyamoto I., Mauro H. *Welding in the World*, **29**, 283 (1991).
17. Prusa J.M., Venkitachalam G., Molian P.A. *Int. J. Mach. Tools Manuf.*, **39**, 431 (1999).
18. Makashev N.K., Asmolov E.S., Blinkov V.V., Boris A.Yu., Buzykin O.G., Burmistrov A.V., Gryaznov M.R., Makarov V.A. *Kvantovaya Elektron.*, **19**, 910 (1992) [*Quantum Electron.*, **22**, 847 (1992)].
19. Grigor'yants A.G., Shiganov I.N., Misyurov A.I. *Tekhnologicheskie protsessy lazernoi obrabotki* (Laser Processing Technology) (Moscow: Izd-vo MGTU im. N.E. Baumana, 2008) p. 524.
20. Poprave R., Weber H., Herziger G. (Eds) *Laser Physics and Applications* (Berlin, Springer-Verlag, 2004).
21. Carslaw H.S, Jaeger J.C. Conduction of Heat in Solids (Oxford: Clarendon Press, 1959; Moscow: Nauka, 1964).
22. Veiko V.P., Libenson M.N., Chervyakov G.G., Yakovlev E.B. *Vzaimodeistvie lazernogo izlucheniya s veshchestvom* (Interaction of Laser Radiation with Matter) (Moscow: Fizmatlit, 2008) p. 175.